

## Hypernuclear Spectroscopy Using the $(e, e'K^+)$ Reaction

L. Yuan<sup>a</sup>, M. Sarsour<sup>b</sup>, T. Miyoshi<sup>c</sup>, X. Zhu<sup>a</sup>, A. Ahmidouch<sup>d</sup>, D. Androic<sup>e</sup>, T. Angelescu<sup>f</sup>,  
 R. Asaturyan<sup>g</sup>, S. Avery<sup>a</sup>, O.K. Baker<sup>a,i</sup>, I. Bertovic<sup>e</sup>, H. Breuer<sup>h</sup>, R. Carlini<sup>i</sup>, J. Cha<sup>a</sup>, R.  
 Chrien<sup>j</sup>, M. Christy<sup>a</sup>, L. Cole<sup>a</sup>, S. Danagoulian<sup>d</sup>, D. Dehnhard<sup>k</sup>, M. Elaasar<sup>l</sup>, A. Empl<sup>b</sup>,  
 R. Ent<sup>i</sup>, H. Fenker<sup>i</sup>, Y. Fujii<sup>c</sup>, M. Furic<sup>e</sup>, L. Gan<sup>a</sup>, K. Garrow<sup>i</sup>, A. Gasparian<sup>a</sup>, P.  
 Gueye<sup>a</sup>, M. Harvey<sup>a</sup>, O. Hashimoto<sup>c</sup>, W. Hinton<sup>a</sup>, B. Hu<sup>a</sup>, E. Hungerford<sup>b</sup>, C. Jackson<sup>a</sup>,  
 K. Johnston<sup>n</sup>, H. Juengst<sup>k</sup>, C. Keppel<sup>a</sup>, K. Lan<sup>b</sup>, Y. Liang<sup>a</sup>, V.P. Likhachev<sup>o</sup>, J.H.  
 Liu<sup>k</sup>, D. Mack<sup>i</sup>, A. Margaryan<sup>g</sup>, P. Markowitz<sup>p</sup>, H. Mkrtchyan<sup>g</sup>, S. N. Nakamura<sup>c</sup> T.  
 Petkovic<sup>e</sup>, J. Reinhold<sup>p</sup>, J. Roche<sup>a</sup>, Y. Sato<sup>c,a</sup>, R. Sawafta<sup>d</sup>, N. Simicevic<sup>n</sup>, G. Smith<sup>i</sup>,  
 S. Stepanyan<sup>g</sup>, V. Tadevosyan<sup>g</sup>, T. Takahashi<sup>c</sup>, K. Tanida<sup>r</sup>, L. Tang<sup>a,i</sup>, M. Ukai<sup>c</sup>,  
 A. Uzzle<sup>a</sup>, W. Vulcan<sup>i</sup>, S. Wells<sup>n</sup>, S. Wood<sup>i</sup>, G. Xu<sup>b</sup>, H. Yamaguchi<sup>c</sup>, C. Yan<sup>i</sup>

(HNSS Collaboration)

<sup>a</sup>Hampton University, Hampton, VA 23668; <sup>b</sup>University of Houston,

Houston, TX 77204; <sup>c</sup>Tohoku University, Sendai,

980-8578, Japan; <sup>d</sup>North Carolina A&T State University,

Greensboro, NC 27411; <sup>e</sup>University of Zagreb,

Zagreb, Croatia; <sup>f</sup>University of Bucharest, Bucharest,

Romania; <sup>g</sup>Yerevan Physics Institute, Yerevan,

Armenia; <sup>h</sup>University of Maryland, College Park,

MD 20742; <sup>i</sup>Thomas Jefferson National Accelerator Facility,

Newport News, VA 23606; <sup>j</sup>Brookhaven National Laboratory,

Upton, NY 11973; <sup>k</sup>University of Minnesota, Minneapolis,

MN 55455; <sup>l</sup>Southern University at New Orleans,

New Orleans, LA 70126; <sup>m</sup>Rensselaer Polytechnic Institute,

Troy, NY 12180; <sup>n</sup>Louisiana Tech University, Ruston,

LA 71272; <sup>o</sup>University of Sao Paulo, Sao Paulo,

Brazil; <sup>p</sup>Florida International University, Miami,

FL 33199; <sup>q</sup>College of William and Mary, Williamsburg,

VA 23187; <sup>r</sup>University of Tokyo, Tokyo 113-0033, Japan

(Dated: November 17, 2018)

## Abstract

A pioneering experiment in  $\Lambda$  hypernuclear spectroscopy, undertaken at the Thomas Jefferson National Accelerator Facility (Jlab), was recently reported. The experiment used the high-precision, continuous electron beam at Jlab, and a special arrangement of spectrometer magnets to measure the spectrum from  $^{nat}\text{C}$  and  $^7\text{Li}$  targets using the  $(e, e'K^+)$  reaction. The  $^{12}_{\Lambda}\text{B}$  spectrum was previously published. This experiment is now reported in more detail, with improved results for the  $^{12}_{\Lambda}\text{B}$  spectrum. In addition, unpublished results of the  $^7_{\Lambda}\text{He}$  spectrum are also shown. This later spectrum indicates the need for a more detailed few-body calculation of the hypernucleus and the reaction process. The success of this experiment demonstrates that the  $(e, e'K^+)$  reaction can be effectively used as a high resolution tool to study hypernuclear spectra, and its use should be vigorously pursued.

PACS numbers: 21.80.+a, 21.10.Dr, 21.60.Cs

Keywords:

## I. INTRODUCTION

The introduction of strangeness into the nuclear medium challenges conventional models of this low-energy, hadronic, many-body system. Of particular interest is the fact that one pion exchange (OPE) between a  $\Lambda$  and a nucleon does not occur due to conservation of isospin. Thus higher mass meson exchanges, including the two-pion exchange coupling of a lambda to a nucleon through an intermediate sigma ( $\Lambda N \rightarrow \Sigma N \rightarrow \Lambda N$ ), is significant, and leads to sizable charge asymmetry and three-body forces[1]. In addition, the strangeness degree of freedom allows the nucleus to rearrange by taking advantage of SU(3) flavor symmetry, in order to maximize the nuclear binding energy[2].

The  $\Lambda$  can also be used as a probe of the nuclear medium. If the  $\Lambda$  is considered a fundamental particle and remains identifiable as such within the nucleus, a hypernuclear  $\Lambda$  will sample the nuclear interior. Thus various features such as  $\Lambda$  decay and  $\Lambda N$  interactions in heavier hypernuclear systems can be extremely interesting. The hypernuclear system can therefore better illuminate features which would be more obscured in conventional nuclear systems.

Also, as it is essentially impossible to directly determine the elementary  $\Lambda$ -Nucleon potential, the  $\Lambda N$  interaction can presently only be extracted from hypernuclei. Fortunately, the  $\Lambda N$  interaction is weak, so that one can with some confidence, obtain a  $\Lambda N$  potential after the effective  $\Lambda$ -Nucleus interaction is found from an analysis of hypernuclear spectra[3]. Such information illuminates the SU(3)<sub>flavor</sub> baryon-baryon interaction at normal nuclear densities. This information can then serve as a normalization point, to extrapolate the interaction to matter-densities found in neutron stars, where mixtures of nucleons and hyperons could form a stable system[4].

Traditionally, hypernuclei have been produced with secondary beams of kaons or pions, as shown in Figure 1a. Because the  $(K^-, \pi^-)$  reaction is exothermic, the momentum transfer to the  $\Lambda$  can be chosen to be small. In this situation the cross section to substitution states ( *i.e* states where the  $\Lambda$  acquires the same shell quantum numbers as those of the neutron which it replaces) is relatively large. On the other hand, the  $(\pi^+, K^+)$  reaction has momentum transfers comparable to the nuclear Fermi-momentum, and the cross section preferentially populates states with high angular momentum transfers [5, 6]. Neither of these two reactions has significant spin-flip amplitude at forward angles where the cross sections

are experimentally accessible. Thus all these spectra are dominated by transitions to natural parity states.

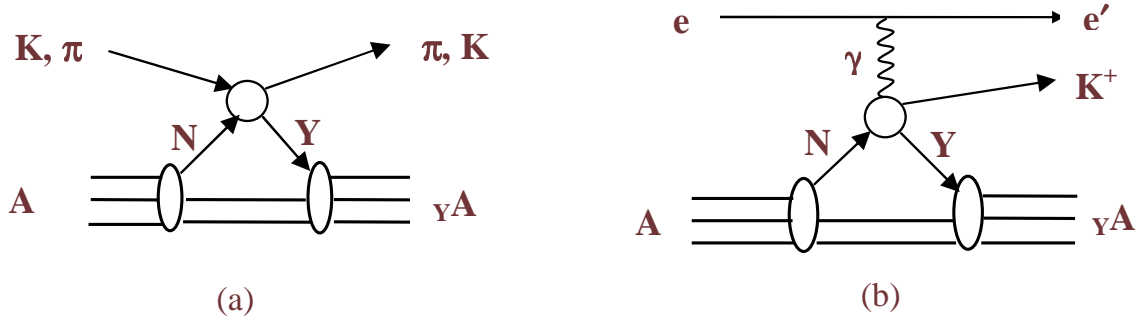


FIG. 1: A schematic representation of the a) mesonic and b) electromagnetic production processes

Aside from early emulsion experiments, mesonic production of hypernuclei has generally provided hypernuclear spectra with energy resolutions  $\geq 2$  MeV. This is due to the intrinsic resolutions of secondary mesonic beamlines, and the target thicknesses required to obtain sufficient counting rates. One previous study did achieve a spectrum resolution of approximately 1.5 MeV for the  ${}_{\Lambda}^{12}\text{C}$  hypernucleus, using a thin target and devoting substantial time to data collection[7]. This work demonstrated the importance of good resolution, as significantly new information, showing some of the fine structure in the  ${}_{\Lambda}^{12}\text{C}$  spectrum, was obtained.

Although, specific hypernuclear states below nucleon emission threshold can be located within a few keV by detecting de-excitation gammas[8, 9] in coincidence with a hypernuclear production reaction, such experiments become more difficult in heavier systems due to the number of transitions which must be unambiguously assigned in an unknown spectrum. It should be noted however, that resolutions of a few hundred keV are also sufficient for many studies, since reaction selectivity and angular dependence potentially allows extraction of the spectroscopic factors to specific states[10]. Of course, a reaction also provides a full spectrum of states which can be clearly identified with a specific hypernucleus. Indeed the excitation strength of the spectrum is of interest, as it directly relates to the model that the reaction proceeds through the interaction of the incident projectile with an identifiable nucleon within the nuclear medium. Thus as an example apropos to the experiment reported here, if the theoretical spectrum does not reproduce the experimental one, it is possible that propagator

re-normalization within the medium could be significant [11], requiring a modification of the single particle picture of the reaction.

Electroproduction of hypernuclei is illustrated by Figure 1b. Electroproduction traditionally has been used for precision studies of nuclear structure, as the exchange of a colorless photon can be accurately described by a first order perturbation calculation. In addition, electron beams have excellent spatial and energy resolutions. Previously, electron accelerators had poor duty factors, significantly impairing high singles rate, coincidence experiments. However, modern, continuous beam accelerators have now overcome this limitation, and although the cross section for kaon electroproduction is some 2 orders of magnitude smaller than hadronic reactions, this can be compensated by increased beam intensity. Targets can be physically small and thin (10-50 mg/cm<sup>2</sup>), allowing studies of almost any isotope. The potential result for  $(e, e'K^+)$  experiments, is an energy resolution of a few hundred keV with reasonable counting rates up to at least medium weight hypernuclei[12].

The  $(e, e'K^+)$  reaction, because of the absorption of the spin 1 virtual photon, has high spin-flip probability even at forward angles. In addition the momentum transfer is high, approximately 300 MeV/c at zero degrees for 1500 MeV incident photons, so the resulting reaction is expected to predominantly excite spin-flip transitions to spin-stretched states of unnatural parity[13]. These states are not strongly excited in hadronic production, and the electromagnetic process acts on a proton rather than a neutron creating proton-hole,  $\Lambda$ -particle states, charge symmetric to those previously studied with meson beams. Precision experiments, comparing mirror hypernuclei, are needed in fact, to extract the charge asymmetry in the  $\Lambda N$  potential.

An initial experiment[14], in Hall C at Thomas Jefferson National Acceleration Facility (Jlab) has been previously reported. The unique features of this experiment include;

1. resolutions of less than 1 MeV FWHM;
2. spectra using the  $(e, e'K^+)$  reaction for the first time;
3. spectra which show unnatural parity (spin flip) states;
4. isospin mirrored spectra compared to those produced by the  $(K^-, \pi^-)$  and  $(\pi^+, K^+)$  reactions;
5. thin targets and low luminosities; and

6. a high-rate silicon strip detector mounted in the focal plane of the electron spectrometer.

This paper discusses the experiment in more detail, and presents an improved spectrum of the  ${}_{\Lambda}^{12}\text{B}$  hypernucleus as well as a previously unpublished spectrum of the  ${}^7\text{Li}(e, e' K^+)_{\Lambda}^7\text{He}$  reaction.

## II. EXPERIMENTAL DETAILS

In electroproduction, the  $\Lambda$  and  $K^+$  particles are created associatively via an interaction between a virtual photon and a proton in the nucleus,  $p(\gamma, K^+)\Lambda$ . The hypernucleus,  ${}_{\Lambda}A$ , is formed by coupling this  $\Lambda$  to the residual nuclear core,  $(Z-1)$ , as shown in Figure 1(b). In electroproduction, the energy and momentum of the virtual photon are defined by  $\omega = E(e) - E(e')$  and  $\vec{q} = \vec{p}(e) - \vec{p}(e')$ , respectively. The four-momentum transfer of the electron is then given by  $Q^2 = q^2 - \omega^2$ . Since the elementary cross section, and the nuclear form factor, fall rapidly with increasing  $Q^2$ , experiments must be done within a small angular range around the direction of the virtual photon. In addition as discussed below, the virtual photon flux is maximized for an electron scattering angle near zero degrees. Thus the experimental geometry requires two spectrometer arms, one to detect the scattered electron and one to detect the kaon, both placed at extremely forward angles.

The electroproduction cross section can be expressed [15] by;

$$\frac{\partial^3 \sigma}{\partial E'_e \partial \Omega'_e \partial \Omega_k} = \Gamma \left[ \frac{\partial \sigma_T}{\partial \Omega_k} + \epsilon \frac{\partial \sigma_L}{\partial \Omega_k} + \epsilon \cos(2\phi) + \cos(\phi_k) \sqrt{2\epsilon(1+\epsilon)} \frac{\partial \sigma_L}{\partial \Omega_k} \right].$$

The factor,  $\Gamma$ , is the virtual flux factor evaluated with electron kinematics in the lab frame. It has the form;

$$\Gamma = \frac{\alpha}{2\pi^2 Q^2} \frac{E_\gamma}{1-\epsilon} \frac{E'_e}{E_e}.$$

In the above equation,  $\epsilon$  is the polarization factor;

$$\epsilon = \left[ 1 + \frac{2|\mathbf{k}|^2}{Q^2} \tan^2(\Theta_e/2) \right]^{-1}.$$

For those virtual photons almost on the mass shell,  $Q^2 = p_\gamma^2 - E_\gamma^2 \rightarrow 0$ . The label on each of the cross section expressions ( $T$ ,  $L$ ,  $P$ , and  $I$ ) represent transverse, longitudinal, polarization, and interference terms. For real photons of course,  $Q^2 \rightarrow 0$ , so only the transverse cross section is non-vanishing, and for the experimental geometry used here, the cross section is completely dominated by the transverse component. Thus the electroproduction cross section may be replaced, to good approximation, by the photoproduction value times the flux factor.

Experimentally,  $\Gamma$  is integrated over the angular and momentum acceptances of the electron spectrometer. In order to maximize the cross section of the elementary,  $p(\gamma, k^+)\Lambda$  reaction, the photon energy is chosen to be about 1.5 GeV. In addition, to keep strangeness production limited essentially to kaons and  $\Lambda$ s, the energy,  $E(e)$ , of the incident electron is set to be  $\approx 1.8$  GeV. In this way, backgrounds from unwanted reactions are reduced. This also allows a physically small, low-momentum electron spectrometer to be employed, as the scattered electron energy,  $(E'_e)$ , is about 0.3 GeV.

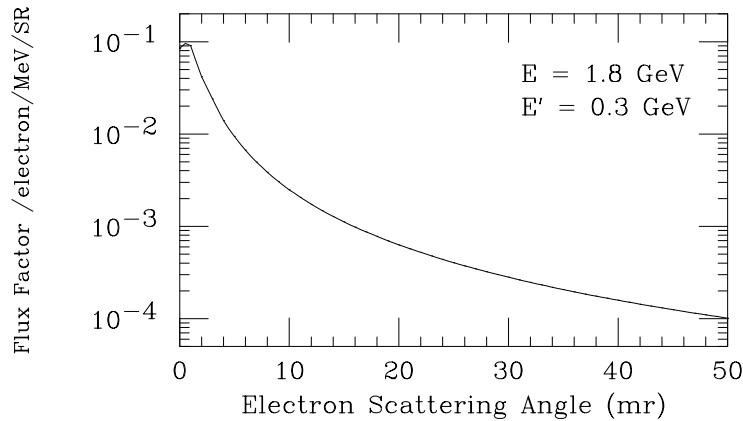


FIG. 2: The virtual photon flux factor as a function of the electron scattering angle

Figure 2. shows the calculated virtual photon flux factor in units of photons per electron per MeV-sr for the chosen kinematics. This flux factor peaks at zero degrees and falls rapidly

as the scattering angle increases[16, 17]. With electrons detected at zero degrees, a large percentage of the scattered electrons are captured by even a small solid angle, increasing the coincidence probability between these electrons and the reaction kaons of interest. In addition, because of the small beam spot ( $\approx 100\mu\text{m}$ ), the  $\approx 0^\circ$  electron scattering angle, and the small momentum value of the scattered electron, it is sufficient to only measure the electron position on the spectrometer focal plane to ensure excellent energy resolution. However, the disadvantage of this geometry is a high electron background rate from target bremsstrahlung, which ultimately limits the usable beam luminosity.

Once the choice of the incident and scattered electron momenta are fixed, the reaction kaon momenta are determined by the kaon reaction angle. In this experiment, the chosen kinematics produced a kaon momenta of  $\approx 1.2\text{GeV}/c$ , providing a 3-momentum transfer of  $\approx 300\text{MeV}/c$  to the recoiling  $\Lambda$ . The kaon momentum provides a reasonable kaon survival fraction, and allows  $\pi/K$  discrimination using threshold aerogel Cerenkov detectors coupled with time of flight. Figure 3 shows a schematic view of the experimental layout.

### A. The Beam

The beam has a bunch width of 1.67 ps with a bunch separation of 2 ns. While the absolute value of the energy of the incident electrons was unimportant (although for kinematic reasons to be discussed below, it did need to be determined), it was extremely important to precisely maintain whatever this energy was over the several weeks of the experiment. Thus the beam momentum is locked by a Fast Feedback Energy Lock System installed in an arc of the accelerator. This system measured, at a repetition rate of 1 khz, the beam parameters at the entrance, the position of maximum momentum dispersion, and the exit of the arc, to extract an energy correction factor. This correction was then applied to the last cavity of the accelerator, maintaining a constant beam energy. The feedback lock controlled the total energy of the primary electron beam to a  $\delta p/p \leq 10^{-4}$ . The intrinsic energy spread in the beam was controlled by a tune of the injector. A similar lock system maintained the beam position on target within  $100\mu\text{m}$ . Although the intrinsic spot size was tuned to be  $\leq 100\mu\text{m}$ , the beam was de-focused to  $4 \times 4\text{ mm}^2$  by a fast raster when incident on the  $\text{CH}_2$  target, to reduce beam heating.

Beam intensities were set to produce an acceptable signal to accidental ratio, which for

the C target was approximately  $0.6 \mu\text{A}$ , or an experimental luminosity of approximately  $4 \times 10^{33} \text{ cm}^{-2}\text{-s}^{-1}$ . Due to the lower radiation length of the  ${}^7\text{Li}$  target, a higher beam current of about  $0.8 \mu\text{A}$  was used. To protect the  $\text{CH}_2$  target, the beam current was kept below  $1.5 \mu\text{A}$ .

Finally, to satisfy conflicting beam requirements when simultaneously operating several experiments in the different experimental Halls, data had to be acquired at two time periods using two different beam energies, 1721 and 1864 MeV. These different energy data were analyzed separately, but the kinematical conditions for the two beam energies were close, and the spectra showed no energy dependence within statistics. Therefore these data were summed after separate analysis to increase the statistical significance of the final spectrum. In addition to calibrations, about 400 hours of data were collected with the  ${}^{nat}\text{C}$  target and about 120 hours with the  ${}^7\text{Li}$  target.

## B. The Splitting Magnet and Targets

In order to detect both scattered electrons and positively charged kaons near zero degrees, a ‘‘C’’ magnetic dipole (splitter) was used. The target was positioned at the upstream side of the effective field boundary of this magnet. The splitter respectively deflected electrons scattered at approximately 0 degrees and kaons at approximately 2 degrees by 33 and 16 degrees, respectively.

Three different, target foils were employed,  $\text{CH}_2$ ,  $8.8 \text{ mg/cm}^2$ ,  ${}^{nat}\text{C}$ ,  $22 \text{ mg/cm}^2$ , and  ${}^7\text{Li}$ ,  $19 \text{ mg/cm}^2$ . By observing the  $p(e, e'K^+)\Lambda$  and  $p(e, e'K^+)\Sigma$ , the hydrogen in the  $\text{CH}_2$  foil was used for energy calibration and optimization of the spectrometer optics. These procedures are described in the subsections below.

## III. THE KAON SPECTROMETER

A short orbit spectrometer (SOS) is one of two existing magnetic spectrometers in Hall C at Jlab, and as it has a flight path of  $\approx 10\text{m}$ , this spectrometer is particularly useful for the detection of particles with short half-lives. However, it has low dispersion and large momentum acceptance, and these characteristics are not well matched to the present experimental geometry. Still the SOS was mounted at the Hall C pivot and had the sophis-

ticated particle identification (PID) package[18] required to identify kaons within the large background of pions and positrons, so it was chosen as the kaon spectrometer for this first ( $e, e'K^+$ ) experiment. It was expected that the overall resolution would be dominated by this spectrometer[22].

The solid angle acceptance of the splitter/SOS spectrometer system was approximately 5 msr, covering a range of scattering angles from 0 to 4 deg. The error in the reconstructed scattering angle was about 13 mr (FWHM), and was dominated by the horizontal angular error measurement. This contributed about 200 keV to the missing mass resolution when the recoil atomic number was  $\geq 6$ . The central momentum of the SOS was set to 1.2 GeV/c. The acceptance was  $\approx 46\%$ , but only the central  $\pm 15\%$  was useful. This acceptance was nearly flat within the missing mass range of interest.

The standard SOS detector package was used. It consisted of: 1) two sets of tracking chambers separated by 0.5 meters; 2) four scintillation hodoscope planes; 3) one aerogel Cerenkov (AC) counter with an optical index of 1.03; 4) one Lucite, total internally reflecting Cerenkov (LC) counter with index 1.49; 5) one gas Cerenkov (GC) detector; and 6) 3 layers of lead-glass shower counters. The tracking detectors were used to determine the position and angle of the particle on the focal plane, and by projection, its scattering angle from the target. The scintillator hodoscopes were used to localize tracks in the wire chambers, and to obtain timing and time of flight (TOF) information for PID. The aerogel Cerenkov detector was used to veto pions and positrons, and the Lucite counter was used to remove protons by tagging high-beta particles. The gas Cerenkov detector and the lead-glass shower counters were used to remove positrons.

### A. The Electron Spectrometer

The scattered electrons were detected in a split-pole, magnetic spectrometer[19], which was well matched to the geometrical kinematics and acceptances. The spectrometer coupled with the phase space of the incident beam, had the capability of obtaining  $5 \times 10^{-4}$  resolution (FWHM  $\delta p/p$ ). The central momentum was chosen to be 300 MeV/c with a momentum acceptance of  $\approx 120$  MeV/c. The solid angle acceptance of the combined splitter/split-pole system was about 9 msr, which effectively tagged about 35% of the virtual photon flux. This provided a spread in the photon flux momentum of  $\approx 120$  MeV/c, centered around

$\approx 1500 \text{ MeV}/c$ . In summary, the geometry of the electron arm was possible because of the excellent phase space of the incident electron beam, the thin targets which limited multiple scattering, and the extremely forward peaking of the virtual photon flux factor.

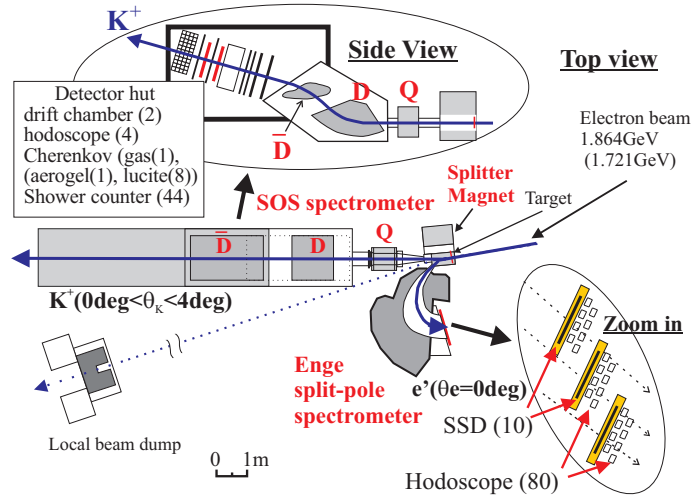


FIG. 3: The experimental plan view showing both the kaon spectrometer (SOS) and the electron spectrometer (ENGE). The SOS is a QDD spectrometer with Q an entrance quadrupole, and DD two dipoles bending in opposite directions, providing large momentum acceptance but reducing dispersion.

However, target bremsstrahlung also peaks at zero degrees and large numbers of scattered electrons are expected to enter the split-pole spectrometer[16]. In fact the experimental luminosity was set by accepting a total rate of  $\approx 2 \times 10^8 \text{ s}^{-1}$  on the instrumented portion of the focal plane. To operate at this rate, the detection system required that only the focal plane position of a scattered electron was needed to obtain the required resolution, since more detailed tracking would have been very inefficient. The focal plane detector[20] was composed of 10, one-dimensional silicon strips segments (SSD), each having 144 strips with a pitch of 0.5mm. These segments were placed approximately perpendicular to the electrons, which were incident at  $\approx 47^\circ$  on a 72 cm length of the focal plane. The singles rate per strip was on average  $\approx 10^5 \text{ s}^{-1}$ .

A set of 8 scintillation strip counters in a hodoscope arrangement were positioned directly behind each of the SSD segments. These strips were 1cm wide, 6cm long and 0.4 cm thick, viewed at one end through a light guide by a 3469 Hamamatsu photomultiplier. Rates per scintillator were found to be  $\leq 1.5 \times 10^6 \text{ hz}$ , and no change in time resolution was observed

up to rates  $\leq 2.5 \times 10^6$  hz. The SSD provided the position of an electron event to within 500  $\mu\text{m}$  and the scintillation hodoscope provided event timing to 250 ps ( $\sigma$ ).

### **B. Pion/Kaon Discrimination**

It was expected that the numbers of positrons, pions and protons in the SOS would be very much larger than the number of kaons. Indeed the measured flux per second of positrons, pions, protons, and kaons from the C target, was  $10^5$ ,  $1.4 \times 10^3$ , 140, and 0.4, respectively. Therefore excellent particle identification was required, not only in the analysis, but also in the hardware trigger.

The standard SOS detector package was used to identify kaons, and its description and operation have been previously discussed[18]. The large flux of positrons was due to the acceptance of scattering angles down to zero degrees, where positrons from Dalitz pairs, created in the target, were observed. Positrons were easily identified and could have been removed in the trigger by the lead-glass shower counter, but detection of the Dalitz pairs provided a useful confirmation of the experimental resolution.

The coincident time resolution between an electron and a kaon was 230 (FWHM) ps, after pulse height and path length corrections were applied. Coupled with a measure of the kaon time-of-flight, the system time resolution was sufficient to identify the real and accidental coincidence peaks, and the true kaon coincident events were selected by a two-dimensional cut on a real coincidence window of 2 ns as shown in Figure 4. Events selected from an average of eight nearby accidental coincidence windows were used to obtain the shape and magnitude of the accidental background spectrum.

### **C. The Expected System Resolution**

Since the entire beamline/spectrometer system was under vacuum, multiple scattering in the air and vacuum windows occurred only at the exit of the spectrometers. Vacuum windows were located immediately before the first tracking detectors so that this effect on the measured track-position was minimized. Table 1 lists the expected contributions to the energy resolution. As discussed above, the contribution from the SOS spectrometer was expected to dominate.

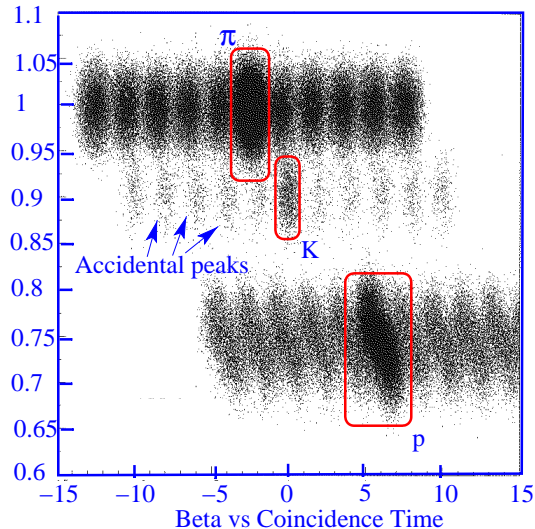


FIG. 4: A plot of SOS particle velocity vs the electron-kaon time-of-flight showing the separation of pions, kaons and protons

TABLE I: Contributions to the System Energy Resolution

Source	Contribution	Resolution (keV)
Beam Energy	$10^{-4}$	$\leq 180$
SOS momentum	$5.5 \times 10^{-4}$	$\approx 660$
Split-pole	$5 \times 10^{-4}$	150
Kaon Scattering Angle ( $^{12}C$ )	13 mr	$\approx 200$
Target Energy Loss ( $^{12}C$ )	1.7 keV/mg/cm <sup>2</sup>	38
Total		$\approx 757$

The system resolution could be experimentally checked using Dalitz pairs from the  $A(e, e'; (e^+e^-))A$  reaction, where both electrons were detected in the electron spectrometer and the positron in the kaon spectrometer. As the electrons and positrons are emitted essentially at zero degrees and the electron mass is negligible, the sum of the separate energies of these particles is equal to the beam energy. The width of the reconstructed beam-energy peak is about 815 keV (FWHM). Unfortunately the kinematics limited the electron pair to the upper region of the momentum acceptance, where the resolution is maximized. From an optical study of the resolution over the entire focal plane, we estimate that the reconstructed

Dalitz pair should be approximately 900 keV (FWHM). This width provides an estimate of the experimental resolution which is due to the detection of only two rather than three particles, but over the full momentum acceptance. The experimental Dalitz pair spectrum is shown in Figure 5.

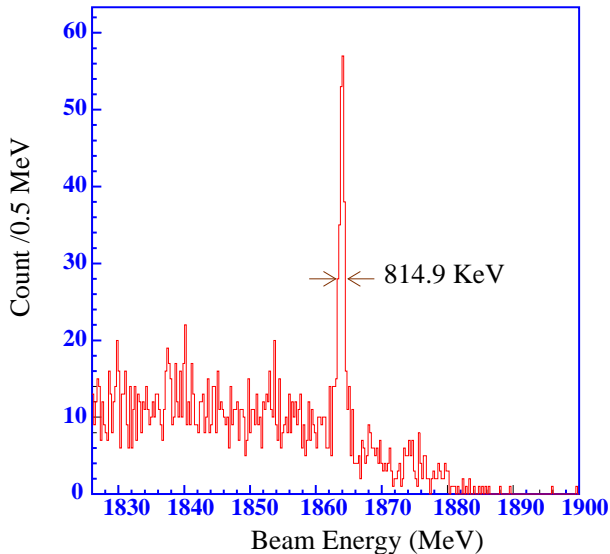


FIG. 5: Reconstructed beam energy from the measurement of Dalitz pairs detected by the spectrometer system. As described in the text, this was used to confirm the energy resolution of the experiment.

#### D. Rates and Background

The singles rate in the electron arm was set to about  $2 \times 10^8 \text{ s}^{-1}$ . As discussed previously, this rate was primarily a result of bremsstrahlung electrons. Therefore, the experimental trigger was the much less frequent identification of a kaon in the kaon spectrometer. The coincidence spectra were then obtained later in off-line analysis. The positrons from  $e^+/e^-$  pair production dominated the rate in the kaon spectrometer. These Dalitz pairs were produced essentially at 0 degrees, and since the SOS acceptance covered 0 to 4 degrees, they were accepted into the spectrometer. However, the combined use of vetoes from AC, GC, and shower counters substantially reduced events triggered by positrons, and they were completely eliminated in the off-line analysis. Rates from protons and pions were

also reduced to approximately 1 kHz after on-line cuts by the AC and LC detectors. The remaining protons and pions were also eliminated in the off-line analysis.

About 95% of the background observed in the raw spectra was due to accidental coincidences. An evaluation of this background began by obtaining a spectrum of the time difference between the emission of the kaon and electron(s) in an event. This time spectrum contained both the real, and a number of accidental peaks, separated by the 2ns time structure in the beam. The summation of the analyzed spectra from 8 of the accidental time-peaks provided a higher statistics measurement of the accidental background. The remaining background (5%) was due to real coincidences of pions (misidentified kaons) with electrons. The TOF path length separation between pions and kaons was about 2 ns, and therefore real coincidences could occur between electrons and misidentified pions which were emitted 2 ns later but arrived in the time window of the real kaon peak. The shape of the pion background in the missing-mass spectra was obtained by cutting on pions in the PID and analyzing coincident pions assuming  $(e, e'K^+)$  kinematics. The absolute magnitude of this background was then obtained by normalizing the pion spectrum to the number of background events.

In addition, the time resolution of  $\sigma \approx 230$  ps, allowed the tails of the real kaon coincidence peak to overlap with an accidental neighbor. Thus to calculate the cross section, the number of true coincident kaons lost from the real time peak was compensated by a cut-efficiency factor.

### **E. Calibrations, Spectrometer Optics, and Kinematics**

Analysis of the experiment required knowledge of the magnetic transport coefficients of the spectrometers. Although the coefficients for the SOS transport had been previously established in several experiments, the addition of the splitting magnet to the system required that they be re-determined. For example, the angular acceptance of the SOS, normally 7 msr for a point target, was reduced to 5 msr by the splitter.

The reconstructed missing mass of a hypernuclear state is a function of the beam energy, the momenta of the scattered electron and kaon, and the scattering angles. In a two-dimensional space defined by the electron and kaon momenta, the recoil missing mass is obtained by a projection of the events onto a locus line. Using an incorrect value of the beam

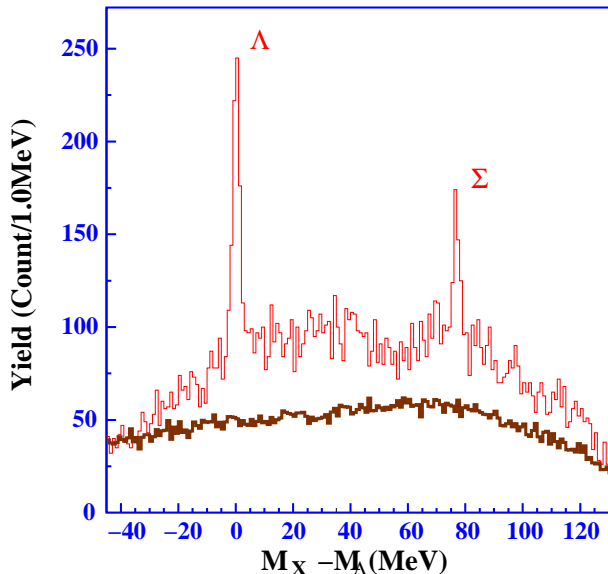


FIG. 6: The missing mass spectrum obtained from a  $\text{CH}_x$  target showing both  $\Lambda$  and  $\Sigma$  production from hydrogen in the target. The solid histogram is the accidental background.

energy or central momentum for either spectrometer arm, results in an incorrect position and slope of this locus line. Therefore there is both an incorrect kinematic position and width for various missing masses. Thus we not only need the relative values of scattering angles and the fractional change of the scattered momentum with respect to central momenta, but also the absolute values of the beam energy and central momenta of the spectrometers, or the absolute values of the scattering angles of the coincident particles. We have now obtained better calibration parameters than those used in the analysis of our previously reported  $^{12}\Lambda\text{B}$  spectrum. The newer analysis reported here improved the missing mass resolution, and more significantly, reduced the tails of the spectral peaks.

The simulation of charged particle trajectories through the system of magnets and detectors used the program, RAYTRACE[21], and the coefficients of the RAYTRACE code were determined by adjusting the splitter contribution so that the calculated multi-dimensional, phase-space distributions from a point beam matched those measured when the entrance angles and positions of reaction protons and pions from the target were restricted by a set of appropriately positioned holes in a tungsten plate (sieve slit) located between the splitting magnet and the SOS[22]. Optimization of the SOS coefficients used a  $\chi^2$  minimization process defined by the difference between the simulated and observed experimental patterns.

The calibration procedure used an initial set of transport parameters for the SOS-splitter spectrometer, and an initial focal plane calibration for the ENGE spectrometer. Then an adjustment to the beam energy and central momentum of the spectrometers was used to simultaneously match the correct kinematic positions and widths of the  $\Lambda$  and  $\Sigma$  peaks as produced in the  $p(\gamma, K^+)Y$  reaction, Figure 6. The fit was also subject to the requirement that a reasonable position and width for the excitation of the ground state doublet was obtained in the  $^{12}C(\gamma, K^+)_{\Lambda}^{12}B$  reaction. This later constraint removed ambiguities in the global parameter space of reconstruction coefficients, but did not place specific conditions on the ground state splitting, excitation strength, or binding energy. It only constrained these observables to lie within an expected range of permissible values[23].

After obtaining a consistent set of absolute beam energy and central momentum values, the transport coefficients were re-fitted to the sieve slit data and the Enge focal plane calibration was re-determined. Residual mass offsets of  $\leq 200$  keV were obtained, and these were dominated by statistics. The peak widths were in good agreement with a Monte Carlo simulation having the same statistics and background levels as the data.

From this more extensive calibration, the analysis produces peak widths of 2.8 MeV, 2.1 MeV and 0.75 MeV for the  $\Lambda$ ,  $\Sigma$ , and ground state doublet of  $_{\Lambda}^{12}B$ , respectively. The previously reported values[14] were, 3.5 MeV, 2.7 MeV, and 0.90 MeV. It is estimated that the new calibration procedure produces a 300 keV error in the missing mass over the 130 MeV spectrometer acceptance.

The broad distribution above background and below the  $\Lambda$  missing mass as seen in Figure 6 was due to hyperon production from the  $^{nat}C$  in the target. Unfortunately during the extended calibrations runs, the C to H ratio changed so that a direct normalization using the known  $p(\gamma, K^+)\Lambda$  cross section could not be applied.

#### IV. EXPERIMENTAL RESULTS AND DISCUSSION

The experiment obtained data for both  $_{\Lambda}^{12}B$  and  $_{\Lambda}^7He$  hypernuclei. The  $_{\Lambda}^{12}B$  spectrum was reported earlier. Subsequently the spectrometer transport and calibrations have been more extensively studied, as discussed above, with the result that the experimental resolution is now  $\approx 750$  keV (FWHM). The new spectrum is presented below, and in addition, we also show for the first time our  $_{\Lambda}^7He$  results.

### A. Spectroscopy of ${}_{\Lambda}^{12}\text{B}$ Hypernuclei

The binding energy spectrum with background of the  ${}_{\Lambda}^{12}\text{B}$  hypernucleus is shown in Figure 7. Two prominent structures are obvious in the spectrum. The spectrum is similar to that predicted by Motoba, *et al* [24, 25] and by Millener[26]. Reference [25] calculates the excitation strengths in DWIA for the photoproduction process of a kaon at an angle of  $3^\circ$  by a 1.3 GeV photon. Our original publication compared the experimental spectrum to a calculation at  $0^\circ$  and a 1.2 GeV photon energy. The curve in Figure 7 is generated by superimposing Gaussian peaks of the strength and at the energy of each state as obtained from a theoretical prediction. For this superposition, the peak widths are assumed to be 750 keV (FWHM) below and 5 MeV above 15 MeV excitation energy. The background is obtained from a polynomial fit to the averaged accidental background. The positions of the states are taken from ref [26], as this latter spectrum was obtained from an effective p shell  $\Lambda$ -nucleus interaction previously matched to  $(\pi^+, K^+)$  data. The reaction strengths [25] for the low-lying states of  ${}_{\Lambda}^{12}\text{B}$  are shown in Figure 8. This theoretical curve is directly overlaid on (not fitted to) the data.

The major excitations are in good statistical agreement with theory both in position and strength. However, the core excited states, predicted to lie between the major shell excitations, seem to be more weakly excited than predicted. Statistics are not sufficient to discuss this region of the spectrum in detail. In comparison to the earlier, published spectrum [14] of this hypernucleus, the resolution and shape of the ground state doublet is improved, and the fluctuations in the core excited region reduced.

The differential cross section can be calculated as if it were photoproduction, by assuming the virtual photons are massless. This averages the elementary  $(\gamma, K)$  reaction at 1500 MeV over the  $\approx 100$  MeV spread of virtual gamma energies. The weighted average of the cross section measurements for the ground state doublet at the two incident beam energies is,  $140 \pm 17(\text{stat}) \pm 18(\text{sys})$  nb/sr. This value is consistent with the individual values of the separate energy measurements, and also the theoretical photoproduction prediction for this angle and energy [25],  $\approx 138$  nb/sr.

The  $2^-$  component of the ground state doublet is predicted to lie at approximately 150 keV excitation energy, and is expected to be dominant, Figure 8. The resolution (and statistics) is insufficient to identify this splitting. The  $3^+$  p-shell state is also predicted to

dominate the spectrum in the  $\approx 10$  MeV excitation region. While theory indicates the dominant structure at this excitation energy is actually created by the overlap, Figure 8, of the  $2^+$  and  $3^+$  p-shell states[26]. These two states are not as degenerate in other calculated spectra [25] which use slightly different effective parameters. The newer data suggest that this p-shell peak may be broader than first indicated, but statistics limit the ability to draw specific conclusions. The results do demonstrate sensitivity to the effective interaction and the DWIA transition amplitudes.

The binding energy scale is determined from the position of the  $\Lambda$  and  $\Sigma$  peaks in the calibration spectrum. The  ${}^{12}_{\Lambda}\text{B}$  binding energy is found to be  $11.52 \pm 0.35$  MeV and is in agreement with the accepted value [27] obtained from a measurement using emulsion, 11.37 MeV.

To confirm our cross section normalization, the quasi-free component of the experimental spectrum was extracted, and the yield corrected for acceptance and momentum transfer [28]. We obtained 4.2 interacting protons, in agreement with previous measurements [29, 30].

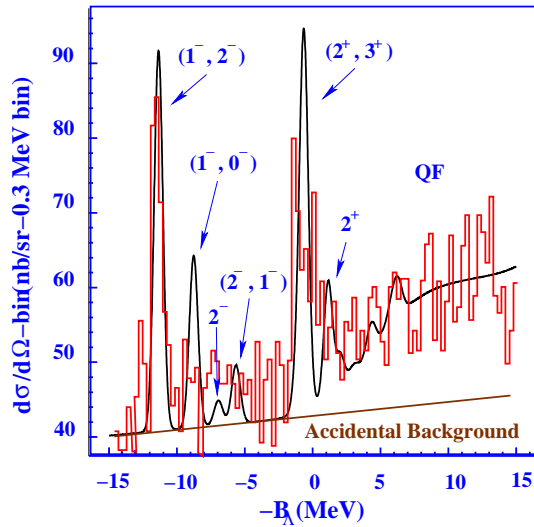


FIG. 7: The binding energy spectrum for  ${}^{12}_{\Lambda}\text{B}$  electroproduced from a  ${}^{nat}\text{C}$  target. The solid histogram is the measured accidental background, and the curve is a theoretical calculation, spread by 750 keV and overlaid on, not fit to, the data.

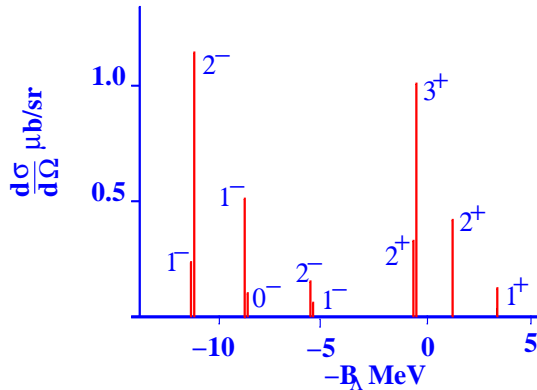


FIG. 8: A schematic representation of the reaction strength for the low lying states of  $^{12}_\Lambda\text{B}$

### B. Spectroscopy of $^7_\Lambda\text{He}$ Hypernuclei

The measured  $^7_\Lambda\text{He}$  spectrum from the  $^7\text{Li}(e, e'K^+)^7_\Lambda\text{He}$  reaction with the accidental background is shown in Figure 9. Data are binned in 1 MeV intervals to improve statistics, although the experimental resolution is comparable to that obtained in the  $^{12}_\Lambda\text{B}$  spectrum (750 keV). The threshold ( $B_\Lambda = 0$ ) is defined as the energy between an unbound  $\Lambda$  and a  $^6\text{He}$  core. Negative energies represent bound  $\Lambda$  states, but in this case the  $^6_\Lambda\text{He} + n$  and  $^5_\Lambda\text{He} + (nn)$  thresholds are some  $\approx 2$  MeV below the threshold value as defined above. The theoretical prediction[31] of the reaction strengths is shown in Figure 10. There is little resemblance to the data, although the experimental statistics are poor. For example there is no evidence of any bound state excitations, although the ground state has a predicted strength of 30 nb/sr. Statistics limit the interpretation of the spectrum as the average statistical error is about 13 nb/sr-MeV between -10 and 0 MeV. Using the expected resolution, the total statistical error in the data is approximately 16 nb/sr summed over a  $4\sigma$  width about the expected ground state position. As discussed in ref. [31, 32], the cluster structure of the  $^7_\Lambda$  hypernuclear system will effect the intrinsic widths of the excited states.

The data suggest a peak at about 7 MeV above the  $\Lambda$ - $^6\text{He}$  threshold, having a statistical uncertainty of about 9% and a width of approximately 3 MeV (FWHM). The background subtracted spectrum with statistical error is shown in Figure 9. If the enhancement at  $\approx 7\text{MeV}$  in the data corresponds to the superposition of the predicted states near 5 MeV and is not a statistical fluctuation, then the energies are incorrect and the strength is somewhat less than predicted. However the widths of these individual states must be due to their

intrinsic values, which are broader than the experimental resolution. Except for the tail of the quasi-free spectrum, no significant features are observed in the data.

The  ${}^7_{\Lambda}\text{He}$  system has two loosely-bound, p-shell neutrons added to a  ${}^4\text{He}$  core. The addition of the  $\Lambda$  should significantly perturb the nuclear core, shrinking the nuclear radius. Such a perturbation is observed in the  ${}^7_{\Lambda}\text{Li}$  hypernuclear system as a change in the  $B(E2)$  gamma transition rate between the 5/2 and 1/2 states[9]. Thus it is expected to find a  ${}^7_{\Lambda}\text{He}$  hypernuclear state[32] bound by about 5 MeV. The ground state masses of the light hypernuclei (s and p shell) are generally determined by the emulsion experiments. In the case of this hypernucleus, the mass distribution from the various emulsion experiments was so broad that a consistent binding energy could not be determined. Isomeric states could explain this broad width[33], as the binding energy is obtained from the energies of the decay products. However this would not effect the widths of the reaction peaks in our experiment. Clearly more experimental investigations are needed, as well as better treatments of the structure of  ${}^7_{\Lambda}\text{He}$  and the  ${}^7\text{Li}(e, e'K^+){}^7_{\Lambda}\text{He}$  reaction mechanism.

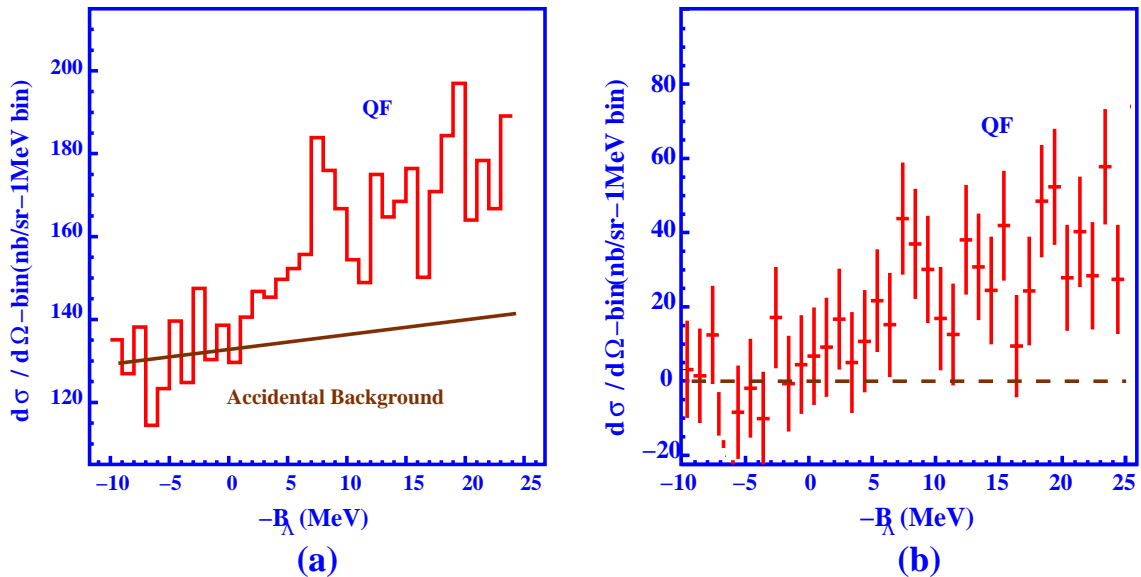


FIG. 9: The binding energy spectrum for  ${}^7_{\Lambda}\text{He}$  electroproduced from a  ${}^7\text{Li}$  target. The data are binned in 1 MeV intervals. In figure (a) the zero in the cross section scale is suppressed. Figure (b) shows the background subtracted spectrum with statistical errors.

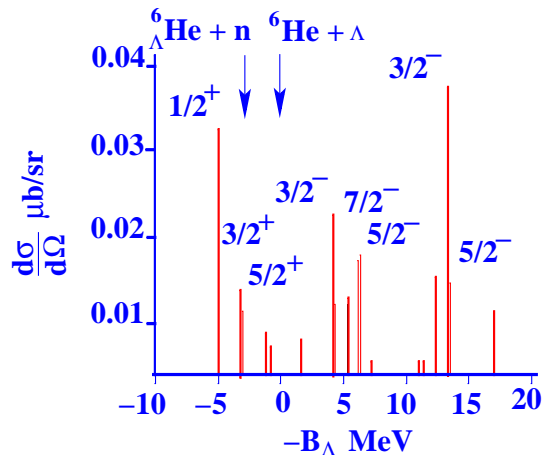


FIG. 10: A schematic representation of the reaction strength for the low lying states of  ${}^7_{\Lambda}\text{He}$ .

## V. CONCLUSION

The first electroproduction experiment using the high quality electron beam at JLab demonstrated a sub-MeV energy resolution. The experiment was carefully crafted to optimize the resolution and rates using the existing SOS magnetic spectrometer. The  ${}^{12}_{\Lambda}\text{B}$  spectrum was similar to that predicted by theory both in the position and magnitude of the major excitations. However the spectrum of  ${}^7_{\Lambda}\text{He}$  was not well reproduced by the existing reaction calculation.

High resolution, systematic studies of electroproduced spectra can complement hypernuclear studies by hadronic probes and gamma spectroscopy. The high-quality electron beam at JLab provides new opportunities for future hypernuclear studies with better resolution and much better quality. A new experiment based on the experience obtained from this experiment is expected to result in resolutions improved by a factor of 2 over the value reported here, with rates increased by a factor of 40. A newly designed Kaon spectrometer will be dedicated to this research [34].

In summary, the investigation of strangeness in nuclear systems is not merely an extension of conventional nuclear physics. Certainly one cannot, nor would one want to, reproduce the wealth of information that has been accumulated on conventional nuclei. The hypernucleus, however, offers a selective probe of the hadronic many-body problem, providing insight in areas that cannot be easily addressed by other techniques. What is now needed is a series of precision studies with high resolution where level positions and weak decay dynamics can

be compared to theory.

### Acknowledgments

Support of the Accelerator and Physics Division staff of the Thomas Jefferson National Accelerator Facility (JLab) is gratefully acknowledged. We wish to thank Dr. D. J. Millener and Dr. T. Motoba for many useful discussions. The Southeastern University Research Association (SURA) operates JLab for the U.S. Department of Energy under Contract No. DE-AC05-84ER40150. This work is also supported in part by research grants from the U.S. Department of Energy and the National Science Foundation, by Monkasho Grant-in-aid for Scientific Research (09304028, 09554007, 12002001), and by the US-Japan collaborative research program under the auspices of the NSF and Japan Society for Promotion of Science.

- 
- [1] Gibson, B.F., and Hungerford III, E.V., *Physics Reports* 257, 349-388 (1995); Gal, A., *Adv. Nucl. Sci.* 8, 1 (1977); Povh, B., *Ann. Rev. Nucl. Part. Sci.* 28, 1 (1978).
  - [2] E. Auerbach, *et al*, *Phys. Rev. Lett.* **47**, 81(1981).
  - [3] D. J. Millener, C. B. Dover, and A. Gal, *Phys. Rev.* **C28**, 2700(1988); T. Motoba, *et al*, *Phys. Rev.* **C38**, (1988); 1322 D. J. Millener, *Nucl. Phys.* **A691**, 93c(2001).
  - [4] M. Prakash, *et al*, *Phys. Rept.* **280**, 1(1997).
  - [5] Milner, C., *et al.*, *Phys. Rev. Lett.* 54, 1237 (1985); Pile, P.H., *et al.*, *Phys. Rev. Lett.* 66, 2585 (1991); Hasegawa, T., *et al.*, *Phys. Rev. Lett.* 74, 224 (1995).
  - [6] Bando, H., Motoba, T., and Yamamoto, Y., *Phys. Rev.* C31, 265 (1985); T. Motoba, *et al*, *Phys. Rev.* **C38**, 1322(1988).
  - [7] T. Hashegawa, *et al.*, *Phys. Rev. Lett.* 74, 224 (1995).
  - [8] Tamura, H., *et al.*, *Phys. Rev. Lett.* 84, 5963 (2000).
  - [9] Tanida, K., *et al.*, *Phys. Rev. Lett.* 86, 1982 (2001).
  - [10] A. S. Rosenthal, *et al*, *Ann. of Phys.* **184**, 33(1988).
  - [11] S. R. Cotanch and S. S. Hsiao, *Nucl. Phys.* **A450**, 419(1986).
  - [12] E. V. Hungerford, *Prog. Theor. Phys. Supp.*, **117**, 135(1994).
  - [13] T. Motoba, M. Stone, and K. Itonaga, *Prog. Theor. Phys. Supp.* **117**, 123(1994); M. Sotona,

- and S. Frullani, *Prog. Theor. Phys. Supp.*, **117**, 151(1994).
- [14] T. Miyoshi, *et al*, *Phys. Rev. Lett.* **90**, 232502(2003)
- [15] T. W. Donnelly, and S. R. Cotanch, *Proceedings of the 1985 CEBAF Summer Study*, 1985; S. S. Hsiao, and S. R. Cotanch, *Phys Rev. C* **28**, 1668 (1983); S. R. Cotanch, and S. S. Hsiao, *Nucl. Phys. A* **450**, 419 (1986).
- [16] G. Xu and E. V. Hungerford, *Nucl. Inst. and Meth.* **A501**,602(2003).
- [17] C. E. Hyde-Wright, W. Bertozzi, and J. M. Finn, *Proc. 1985 CEBAF Summer Workshop*, Newport News, VA, 1985.
- [18] G. Niculescu, *et al*, *Phys. Rev. Lett.*, **81**, 1805(1998).
- [19] J. E. Spencer, and H. A. Enge, *Nucl. Instr. Meth.* **49**, 177 (1967).
- [20] T. Miyoshi, *et.al.*, *Nucl. Instr. and Meth.*, **A496** (2003) 362-372.
- [21] S. Kowalski and H. A. Enge, *Nucl. Inst. and Meth.* **A258**. (1987)407.
- [22] L. Tang, C. Yan, and E. V. Hungerford, *Nucl. Inst. and Meth.* **A366**,259(1995).
- [23] Although Bayesian probability analysis was not directly used here, the application of prior information on allowed values of a likelihood were used in this spirit.
- [24] T. Motoba, M. Sotona, and K. Itonga, *Prog. Theor. Phys. Supp.*, **117**, 123(1994).
- [25] T. Motoba, *Proceedings of the 8<sup>th</sup> Conference on Mesons and Light Nuclei*, J. Adams, ed., *AIP* **603**, 125(2001); and T. Motoba, private communication.
- [26] D. J. Millener, *Proceedings of the Jlab Workshop on Hypernuclear Physics with Electromagnetic Probes*, L. Tang and O. Hashimoto, eds., December 2-4, 1999, Hampton University, Hampton, VA.
- [27] M. Jurić, *Nucl. Phys.* **B52**, 1(1973)
- [28] C. J. Bebek, *et al*, *Phys. Rev.* **D15**,594(1977).
- [29] W. Hinton, PhD dissertation, Hampton University (1999).
- [30] H. Yamazaki, *et al*, *Phys. Rev.*, **C52**, R1157(1995).
- [31] O. Richter, M. Sotona, and J. Žofka, *Phys. Rev.* **C6**, 2753(1991).
- [32] E. Hiyama, *et al*, *Phys. Rev.* **C53**,2075(1996)
- [33] A. Gal, *Adv. Nucl. Phys.*, **8**(1975)1.
- [34] Jlab proposal E01-011, O. Hashimoto, L. tang, and J. Reinhold, spokespersons